Robustness of Image-Based Visual Servoing With a Calibrated Camera in the Presence of Uncertainties in the Three-Dimensional Structure

Ezio Malis, Youcef Mezouar, and Patrick Rives, *Member, IEEE*

***Abstract*—This paper concerns the stability analysis of image-based visual servoing control laws with respect to uncertainties on the 3-D parameters needed to compute the interaction matrix for any calibrated central catadioptric camera. In the recent past, research on image-based visual servoing has been concentrated on potential problems of stability and on robustness with respect to camera-calibration errors. Only little attention, if any, has been devoted to the robustness of image-based visual servoing to estimation errors on the 3-D structure. It is generally believed that a rough approximation of the 3-D structure is sufficient to ensure the stability of the control law. In this paper, we prove that this is not always true and that an extreme care must be taken when approximating the depth distribution to ensure stability of the image-based control law. The theoretical results are obtained not only for conventional pinhole cameras but for the entire class of central catadioptric systems as well.**

***Index Terms*—Image-based, stability analysis, visual servoing.**

I. Introduction

VISUAL servoing is a flexible method for the control of uncalibrated dynamic systems evolving in an unknown environment. Typical applications of visual servoing are positioning of a robot and tracking of objects by using the information provided by an in-hand camera. Several vision-based control laws have been proposed in the literature (see [1] and [2] and the recent tutorial in [3] and [4]). Contrary to model-based visual servoing methods, image-based visual servoing does not need the knowledge of the full model of the target. On the other hand, it is necessary to provide some information about the 3-D structure of the object in the camera frame. In this paper, we consider the case in which the task function is built using the coordinates of image points. Thus, the interaction matrix depends on the depths of the corresponding 3-D points [5]. It is generally believed that a rough approximation of the depths is sufficient to ensure the stability of the control law. However, if the environment is completely unknown and the robot is uncalibrated, the stability of the visual servoing in the presence of depth-estimation errors can become a serious issue. In the recent past, research on the stability of image-based visual servoing has been concentrated on the solution of convergence and visibility problems.

Convergence problems occur since image-based control is a local method that, even in the absence of calibration errors, can fail if the initial camera displacement is too big [6]. In order to avoid these potential convergence problems, several possible approaches have been proposed. In hybrid approaches, some global information is introduced by estimating the camera displacement between the current and reference views [7]–[9]. The rotation of the camera is, thus, controlled directly in the Cartesian space while some image-based information is used to control the translation. The image-based information used in [7] consists of only one image control point. Thus, the method does not need the estimation of the depths of all other points, and it is stable for any positive approximation of the depth of the control point [10]. This approach has been easily extended to the entire class of central catadioptric systems in [11]. Conversely, other hybrid approaches [8] and [9] use all available information in the image, and thus, they need the estimation of the depth distribution. A partitioned approach [12] has been proposed in order to avoid the camera-displacement reconstruction, but the approach is also strongly dependent on the depth-distribution estimation. For this reason, the stability analysis of hybrid (except for [10]) and partitioned approaches is as difficult as the stability analysis of the standard image-based visual servoing. Another solution to potential stability problem of the image-based approach is provided by interpolation approaches. These methods define a path in the image by interpolating initial and reference image features [13], [14]. Thus, the error in the image is maintained small at each iteration of the control law. Even if interpolation approaches are an elegant solution to potential convergence problems of the standard image-based visual servoing, a fundamental theoretical question stands: How is the image-based visual servoing robust with respect to calibration errors? Due to the complexity of the problem, only few theoretical results have been obtained concerning the stability analysis of image-based visual servoing in the presence of calibration errors. The theoretical analysis has been carried out only in very simple cases [15]–[17], often considering a simplified model for the camera-intrinsic parameters but always supposing that the depth distribution was perfectly estimated.

Visibility problems occur since conventional cameras suffer from a restricted field of view. This motivated the growing

Manuscript received June 26, 2008; revised February 24, 2009. First published December 8, 2009; current version published February 9, 2010. This paper was recommended for publication by Associate Editor S. Hirai and Editor L. Parker upon evaluation of the reviewers' comments. This paper was presented in part at the IEEE/RSJ International Conference on Intelligent Robots and Systems, Sendai, Japan, October 2004, and at the IEEE International Conference on Robotics and Automation, Taipei, Taiwan, September 2003.

E. Malis and P. Rives are with the Institut National de Recherche en Informatique et en Automatique, Sophia Antipolis 06902, France (e-mail: Ezio.Malis@sophia.inria.fr; Patrick.Rives@sophia.inria.fr).

Y. Mezouar is with the Laboratoire des Sciences et Matériaux pour l'électronique, University Blaise Pascal, Aubiere 63177, France (e-mail: youcef.mezouar@lasmea.univ-bpclermont.fr).

Digital Object Identifier 10.1109/TRO.2009.2033332

interest for omni-directional sensors in robotics applications. In the literature, there have been several methods proposed to increase the field of view of cameras systems [18]. One effective way is to combine mirrors with a conventional imaging system. The obtained sensors are referred to as catadioptric imaging systems. The resulting imaging systems have been termed central catadioptric when a single projection center describes the world-image mapping. From a practical view point, a single center of projection is a desirable property for an imaging system [19]. Baker and Nayar in [19] derive the entire class of catadioptric systems with a single viewpoint. Many applications in vision-based robotics, such as mobile robot localization [20], [22] and navigation [23], can benefit from a panoramic field of view provided by omni-directional cameras. Clearly, visual servoing applications can also benefit from cameras with a wide field of view since vision-based control methods need to maintain the target visible in the image during the task. As a consequence, such sensors have been successfully integrated as part of a closed-loop feedback-control system [24]–[27]. However, the theoretical stability analysis of image-based control laws has never been done.

The main contribution of this paper is the theoretical study of the robustness of standard image-based visual servoing (i.e., when points coordinates are used as input of the control scheme) with respect to errors on the 3-D parameters introduced in the interaction matrix when any central catadioptric camera is used as a sensor [28], which includes the conventional perspective pinhole cameras [29]. The analysis proposed in this paper is not only limited to standard image-based control laws, but it applies to the efficient second-order approximation method (ESM) control law proposed in [30] as well.

II. Theoretical Background

In this section, we describe the projection model for central catadioptric cameras, and then, we focus on eye-in-hand image-based visual servoing methods.

A. General Camera Model

As shown in [19], a central catadioptric system can be built by combining an hyperbolic, elliptical, or planar mirror with a perspective camera and a parabolic mirror with an orthographic camera. To simplify notations, conventional perspective cameras will be embedded in the set of central catadioptric cameras. In [31], a unifying theory for central panoramic systems is presented. According to this generic model, all central panoramic cameras can be modeled by a central projection onto a sphere followed by a central projection onto the image plane (see Fig. 1).

This generic model can be parameterized by the couple (ξ, φ) describing the type of sensor and the shape of the mirror. Setting $\xi = 0$, the general projection model becomes the well-known perspective-projection model.

Let $\mathcal{F}_c$ and $\mathcal{F}_m$ be the frames attached to the conventional camera and to the mirror, respectively. Suppose that $\mathcal{F}_c$ and $\mathcal{F}_m$ are related by a translation along the Z-axis. The centers C and M of $\mathcal{F}_c$ and $\mathcal{F}_m$ will be called optical center and principal projection center, respectively. Let $\mathcal{X}$ be a 3-D point

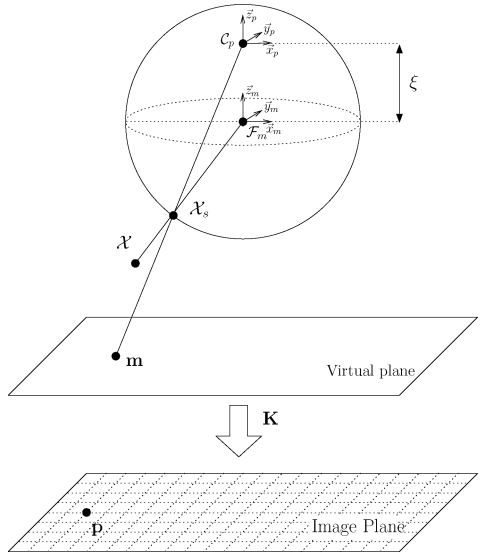

Fig. 1. Generic central catadioptric camera model.

with coordinates $\mathbf{X} = (X,\ Y,\ Z)$ with respect to $\mathcal{F}_m$. After setting $\rho = \sqrt{X^2 + Y^2 + Z^2}$, let $\mathbf{m} = (x, y, 1)$ be the point (in normalized homogeneous coordinated) projected into a virtual plane according to the generic projection model [31]

$$\mathbf{m} = \left(\frac{X}{Z + \xi\rho}, \frac{Y}{Z + \xi\rho}, 1 \right). \tag{1}$$

Taking into account the intrinsic camera and mirror parameters, the 3-D point $\mathcal{X}$ is projected in the real image plane to a point with homogeneous pixel coordinates $\mathbf{p} = (u, v, 1)$

$$\mathbf{p} = \mathbf{K}\mathbf{m} \tag{2}$$

where the upper triangular matrix $\mathbf{K}$ contains the camera intrinsic parameters and the mirror parameter φ. Using approximations $\widehat{\mathbf{K}}$ of the camera and mirror intrinsic parameters $\mathbf{K}$ and a measured image point $\mathbf{p}$, it is possible to compute the corresponding normalized point from (2): $\widehat{\mathbf{m}} = \widehat{\mathbf{K}}^{-1}\mathbf{p}$. Obviously, if the camera and mirror intrinsic parameters are perfectly known $\widehat{\mathbf{K}} = \mathbf{K}$, the normalized coordinates are perfectly estimated $\widehat{\mathbf{m}} = \mathbf{m}$.

B. Interaction Matrix of Central Catadioptric Cameras

Consider a 3-D point $\mathcal{X}_i$ with coordinates $\mathbf{X}_i = (X_i, Y_i, Z_i)$ with respect to $\mathcal{F}_m$ and its normalized image coordinates extracted from $\mathbf{m}$: $\mathbf{s}_i = (x_i, y_i)$. The derivative of $\mathbf{s}_i$ with respect to time is

$$\dot{\mathbf{s}}_i = \mathbf{L}_i \mathbf{v}$$

where $\mathbf{v}$ is the velocity of the camera, and $\mathbf{L}_i$ is the interaction matrix. The interaction matrix can be derived by differentiating the function $\mathbf{f}(\mathbf{X})$ with respect to the camera pose evaluated at the origin or by following [27]. $\mathbf{L}_i$ can be decomposed into two

submatrices $\mathbf{L}_i = [\mathbf{A}_i \ \mathbf{B}_i]$ with

$$\mathbf{A}_i = \begin{bmatrix} -\frac{1+x_i^2(1-\xi(\sigma_i+\xi))+y_i^2}{\rho_i(\sigma_i+\xi)} & \frac{\xi x_i y_i}{\rho_i} & \frac{x_i\sigma_i}{\rho_i} \\ \frac{\xi x_i y_i}{\rho_i} & -\frac{1+x_i^2+y_i^2(1-\xi(\sigma_i+\xi))}{\rho_i(\sigma_i+\xi)} & \frac{y_i\sigma_i}{\rho_i} \end{bmatrix} \tag{3}$$

$$\mathbf{B}_i = \begin{bmatrix} x_i y_i & -\frac{(1+x_i^2)\sigma_i-\xi y_i^2}{\sigma_i+\xi} & y_i \\ \frac{(1+y_i^2)\sigma_i-\xi x_i^2}{\sigma_i+\xi} & -x_i y_i & -x_i \end{bmatrix} \tag{4}$$

where $\sigma_i = \sqrt{1+(1-\xi^2)(x_i^2+y_i^2)}$. Equations (3) and (4) present the general central catadioptric interaction matrix as a function of image coordinates $\mathbf{s}_i$, the distance $\rho_i = \sqrt{X_i^2+Y_i^2+Z_i^2}$, and sensor parameter ξ. Notice that if $\xi = 0$, then the interaction matrix $\mathbf{L}_i$ is the well-known interaction matrix for conventional perspective cameras.

We rewrite the interaction matrix valid for the generic catadioptric model in order to have a structure similar to the structure of the standard perspective interaction matrix.

In the sequel, we assume that $Z \neq 0$. Let us denote $\eta_i = \text{sign}(Z_i)\rho_i/|Z_i| = \text{sign}(Z_i)\sqrt{1+X_i^2/Z_i^2+Y_i^2/Z_i^2}$. The coordinates of the image point can be rewritten as

$$x_i = \frac{X_i/Z_i}{1+\xi\eta_i}$$

$$y_i = \frac{Y_i/Z_i}{1+\xi\eta_i}.$$

By combining the two previous equations, it is easy to show that η_i is the solution of the following second-order equation:

$$\eta_i^2 - (x_i+y_i)^2(1+\xi\eta_i)^2 - 1 = 0$$

with the following potential solutions:

$$\eta_i = \frac{\pm\sigma_i - \xi(x_i^2+y_i^2)}{\xi^2(x_i^2+y_i^2)-1}. \tag{5}$$

Note that the sign of η_i is equal to the sign of Z_i, and then, it can easily be shown that the exact solution is

$$\eta_i = \frac{-\sigma_i - \xi(x_i^2+y_i^2)}{\xi^2(x_i^2+y_i^2)-1}. \tag{6}$$

This equation shows that η_i can be computed as a function of image coordinates $\mathbf{s}_i$ and sensor parameter ξ. The matrix $\mathbf{A}_i$ can thus be rewritten as

$$\mathbf{A}_i = \frac{1}{Z_i}\mathbf{G}_i$$

with

$$\mathbf{G}_i = \begin{bmatrix} -\frac{1+x_i^2(1-\xi(\sigma_i+\xi))+y_i^2}{\eta_i(\sigma_i+\xi)} & \frac{\xi x_i y_i}{\eta_i} & \frac{x_i\sigma_i}{\eta_i} \\ \frac{\xi x_i y_i}{\eta_i} & -\frac{1+x_i^2+y_i^2(1-\xi(\sigma_i+\xi))}{\eta_i(\sigma_i+\xi)} & \frac{y_i\sigma_i}{\eta_i} \end{bmatrix}.$$

Note that, only the depth Z_i is unknown in the matrix $\mathbf{A}_i$. If we consider the $(2n \times 1)$ vector $\mathbf{s} = (\mathbf{s}_1, \mathbf{s}_2, \ldots, \mathbf{s}_n)$, the corresponding $(2n \times 6)$ interaction matrix is $\mathbf{L}(\mathbf{z}, \mathbf{s}) = (\mathbf{L}_1, \mathbf{L}_2, \ldots, \mathbf{L}_n)$, and the time derivative of $\mathbf{s}$ is

$$\dot{\mathbf{s}} = \mathbf{L}(\mathbf{z}, \mathbf{s})\mathbf{v}.$$

Matrix $\mathbf{L}(\mathbf{z}, \mathbf{s})$ can be decomposed into two $(2n \times 3)$ submatrices

$$\mathbf{L}(\mathbf{z}, \mathbf{s}) = [\mathbf{A}(\mathbf{z}, \mathbf{s}) \ \mathbf{B}(\mathbf{s})]$$

where $\mathbf{A} = (\mathbf{A}_1, \mathbf{A}_2, \ldots, \mathbf{A}_n)$, and $\mathbf{B} = (\mathbf{B}_1, \mathbf{B}_2, \ldots, \mathbf{B}_n)$. Due to the form of matrix $\mathbf{A}(\mathbf{z}, \mathbf{s})$, we also have

$$\mathbf{A}(\mathbf{z}, \mathbf{s}) = \mathbf{D}(\mathbf{z})\ \mathbf{G}(\mathbf{s})$$

where $\mathbf{G}(\mathbf{s}) = (\mathbf{G}_1, \mathbf{G}_2, \ldots, \mathbf{G}_n)$, and $\mathbf{D}(\mathbf{z})$ is a $(2n \times 2n)$ diagonal matrix containing the depth distribution $\mathbf{z}$

$$\mathbf{D}(\mathbf{z}) = \text{diag}\left(\frac{1}{Z_1}, \frac{1}{Z_1}, \frac{1}{Z_2}, \frac{1}{Z_2}, \ldots, \frac{1}{Z_n}, \frac{1}{Z_n}\right).$$

C. Image-Based Visual Servoing

The goal of image-based visual servoing is to position a robot by controlling the current position of the robot such that the current measured image features $\mathbf{s}$ reach their reference $\mathbf{s}^*$. Consider the following task function [5]:

$$\mathbf{e} = \mathbf{C}(\mathbf{s} - \mathbf{s}^*)$$

where $\mathbf{C}$ is a $(6 \times 2n)$ combination matrix. Several choices have been proposed for this matrix, as given in the following points.

1) $\mathbf{C} = \widehat{\mathbf{L}}^+$, where $\widehat{\mathbf{L}}^+$ is the pseudoinverse of an approximation of the true $(2n \times 6)$ interaction matrix [5].
2) $\mathbf{C} = \widehat{\mathbf{L}}^+|_{\mathbf{s}=\mathbf{s}^*}$, where the matrix $\widehat{\mathbf{L}}^+$is computed at the reference coordinates and, thus, is constant [5].
3) $\mathbf{C} = (\widehat{\mathbf{L}}^+ + \widehat{\mathbf{L}}^+|_{\mathbf{s}=\mathbf{s}^*})/2$, where the matrix is the average between the previous matrices [30].
4) $\mathbf{C} = \beta\widehat{\mathbf{L}}^+ + (1-\beta)\widehat{\mathbf{L}}^+|_{\mathbf{s}=\mathbf{s}^*}$, where β is a weight such that $0 \leq \beta \leq 1$ [32].

In these cases, the derivative of the task function is

$$\dot{\mathbf{e}} = \frac{d\mathbf{C}}{dt}(\mathbf{s}-\mathbf{s}^*) + \mathbf{C}\dot{\mathbf{s}} = (\mathbf{O}(\mathbf{s}-\mathbf{s}^*) + \mathbf{C}\mathbf{L})\mathbf{v} \tag{7}$$

where $\mathbf{O}(\mathbf{s}-\mathbf{s}^*)$ is a 6×6 matrix such that $\mathbf{O}(\mathbf{s}-\mathbf{s}^*)|_{\mathbf{s}=\mathbf{s}^*} = 0$. Consider the following control law:

$$\mathbf{v} = -\lambda\ \mathbf{e}. \tag{8}$$

In order to compute the control law, it is necessary to provide the approximated interaction matrix $\widehat{\mathbf{L}}$. Plugging (8) into (7), we obtain the following closed-loop equation:

$$\dot{\mathbf{e}} = -\lambda(\mathbf{O}(\mathbf{s}-\mathbf{s}^*) + \mathbf{C}\mathbf{L})\mathbf{e}. \tag{9}$$

It is well known from the control theory that the equilibrium point $\mathbf{e} = 0$ of the nonlinear system (9) is locally asymptotically stable in a neighborhood of $\mathbf{s} = \mathbf{s}^*$, if and only if the equilibrium point of the linearized system is stable

$$\dot{\mathbf{e}} = \lambda\mathbf{Q}\mathbf{e} \tag{10}$$

where $\mathbf{Q} = -(\mathbf{C}\mathbf{L})|_{\mathbf{s}=\mathbf{s}^*} = -\widehat{\mathbf{L}}^+(\mathbf{s}^*)\mathbf{L}(\mathbf{s}^*)$ for any of the four choices of $\mathbf{C}$. The equilibrium point of the linear system (10) is asymptotically stable *if and only if* $\mathbf{Q}$ has eigenvalues with negative real part

$$\text{real}(\text{eig}(\mathbf{Q})) = \text{real}(\text{eig}(-\widehat{\mathbf{L}}^+\mathbf{L})) < 0.$$

The matrix $\mathbf{Q} = \mathbf{Q}(\widehat{\mathbf{K}}, \mathbf{K}, \widehat{\mathbf{M}}, \mathbf{m}, \widehat{\mathbf{z}}, \mathbf{z})$ depends on two sets of unknown parameters. Obviously, if $\mathbf{K} = \widehat{\mathbf{K}}, \widehat{\mathbf{M}} = \mathbf{m}$ and $\widehat{\mathbf{z}} = \mathbf{z}$, then $\mathbf{Q} = \mathbf{I}$, and the system is stable. The objective of the robustness analysis is to know if the system is locally asymptotically stable in the presence of unavoidable calibration errors.

III. Stability Analysis

Let us suppose that the camera and mirror parameters are perfectly known (i.e., $\widehat{\mathbf{K}} = \mathbf{K}$, $\widehat{\mathbf{m}} = \mathbf{m}$). Thus, the normalized points are perfectly estimated $\widehat{\mathbf{s}} = \mathbf{s}$, and the uncertainties on the estimated interaction matrix only depend on the depth distribution $\widehat{\mathbf{z}}$

$$\widehat{\mathbf{L}}(\widehat{\mathbf{z}}, \mathbf{s}) = [\, \mathbf{A}(\widehat{\mathbf{z}}, \mathbf{s}) \quad \mathbf{B}(\mathbf{s}) \,].$$

It is easy to verify that the estimated submatrix $\mathbf{A}(\widehat{\mathbf{z}}, \mathbf{s})$ can be written as a function of the true submatrix $\mathbf{A}(\mathbf{z}, \mathbf{s})$

$$\mathbf{A}(\widehat{\mathbf{z}}, \mathbf{s}) = \mathbf{D}(\widehat{\mathbf{z}})\ \mathbf{G}(\mathbf{s}) = \mathbf{\Gamma}^{-1}(\widehat{\mathbf{z}}, \mathbf{z})\mathbf{A}(\mathbf{z}, \mathbf{s}) \tag{11}$$

where, setting $\gamma_i = \widehat{Z}_i / Z_i$ as the ratio between the estimated and true depths, the diagonal matrix $\mathbf{\Gamma}$ is

$$\mathbf{\Gamma} = \mathbf{D}(\mathbf{z})\mathbf{D}^{-1}(\widehat{\mathbf{z}}) = \mathrm{diag}\,(\gamma_1, \gamma_1, \gamma_2, \gamma_2, \ldots, \gamma_n, \gamma_n).$$

From (11), one can deduce that

$$\mathbf{L}(\mathbf{z}, \mathbf{s}) = [\, \mathbf{\Gamma}\mathbf{A}(\widehat{\mathbf{z}}, \mathbf{s}) \quad \mathbf{B}(\mathbf{s}) \,].$$

Setting $\mathbf{\Delta} = \mathbf{\Gamma} - \mathbf{I}$ one can deduce that

$$\mathbf{L} = \widehat{\mathbf{L}} + \mathbf{\Delta}\,[\, \mathbf{A}(\widehat{\mathbf{z}}, \mathbf{s}) \quad \mathbf{0} \,].$$

Setting $\widehat{\mathbf{A}} = \mathbf{A}(\widehat{\mathbf{z}}, \mathbf{s})$, the matrix $\mathbf{Q}$ is

$$\mathbf{Q} = -\widehat{\mathbf{L}}^{+}\mathbf{L} = -\mathbf{I} - \left[\, \widehat{\mathbf{L}}^{+}\mathbf{\Delta}\widehat{\mathbf{A}} \quad \mathbf{0} \,\right].$$

If $\widehat{\mathbf{L}}$ is full rank, its pseudoinverse can be written as

$$\widehat{\mathbf{L}}^{+} = \begin{bmatrix} \widehat{\mathbf{A}}^{\natural} \\ \mathbf{B}^{\natural} \end{bmatrix}$$

where $\widehat{\mathbf{A}}^{\natural}$ is a generalized inverse of $\widehat{\mathbf{A}}$ (i.e., $\widehat{\mathbf{A}}^{\natural}\widehat{\mathbf{A}} = \mathbf{I}$), and $\mathbf{B}^{\natural}$ is a generalized inverse of $\widehat{\mathbf{B}}$ (i.e., $\mathbf{B}^{\natural}\mathbf{B} = \mathbf{I}$). Note also that $\widehat{\mathbf{A}}^{\natural}\mathbf{B} = 0$ and that $\mathbf{B}^{\natural}\widehat{\mathbf{A}} = 0$. Matrix $\mathbf{Q}$ can be rewritten as

$$\mathbf{Q} = -\mathbf{I} - \begin{bmatrix} \widehat{\mathbf{A}}^{\natural} \\ \mathbf{B}^{\natural} \end{bmatrix} \left[\, \mathbf{\Delta}\widehat{\mathbf{A}} \quad \mathbf{0} \,\right] = - \begin{bmatrix} \mathbf{I} + \widehat{\mathbf{A}}^{\natural}\mathbf{\Delta}\widehat{\mathbf{A}} & \mathbf{0} \\ \mathbf{B}^{\natural}\mathbf{\Delta}\widehat{\mathbf{A}} & \mathbf{I} \end{bmatrix}.$$

Setting again $\mathbf{\Delta} = \mathbf{\Gamma} - \mathbf{I}$

$$\mathbf{Q} = \begin{bmatrix} \mathbf{Q}_{11} & \mathbf{Q}_{12} \\ \mathbf{Q}_{21} & \mathbf{Q}_{22} \end{bmatrix} = \begin{bmatrix} -\widehat{\mathbf{A}}^{\natural}\mathbf{\Gamma}\widehat{\mathbf{A}} & \mathbf{0} \\ -\mathbf{B}^{\natural}\mathbf{\Gamma}\widehat{\mathbf{A}} & -\mathbf{I} \end{bmatrix}.$$

Thus, the closed-loop matrix is block lower triangular. In this case, it is well known that the eigenvalues of $\mathbf{Q}$ are the eigenvalues of the two (3×3) matrices $\mathbf{Q}_{11}$ and $\mathbf{Q}_{22}$. Since $\mathbf{Q}_{22} = -\mathbf{I}$ its eigenvalues are negative for any choice of the depth distribution. The analysis is limited to the eigenvalues of the following matrix:

$$\mathbf{Q}_{11} = -\widehat{\mathbf{A}}^{\natural}\mathbf{\Gamma}\widehat{\mathbf{A}} = \sum_{i=1}^{n} \gamma_i \widehat{\mathbf{A}}_i^{\natural}\widehat{\mathbf{A}}_i$$

where $\widehat{\mathbf{A}}_i^{\natural}$ are submatrices of matrix $\widehat{\mathbf{A}}$. Note that

$$\widehat{\mathbf{A}}^{\natural}\widehat{\mathbf{A}} = \sum_{i=1}^{n} \widehat{\mathbf{A}}_i^{\natural}\widehat{\mathbf{A}}_i = \mathbf{I}.$$

The first important results of the analysis is that *the depth distribution can be estimated up to a positive scalar factor.* The scalar factor only influence the performance of the servoing but not its stability since it does not change the sign of the eigenvalues. Thus, without loss of generality, we can factor $\gamma_j > 0$ from the sum

$$\mathbf{Q}_{11} = -\gamma_j \sum_{i=1}^{n} \psi_i \widehat{\mathbf{A}}_i^{\natural}\widehat{\mathbf{A}}_i = \gamma_j \mathbf{F}$$

where $\psi_i = \gamma_i / \gamma_j$, and obviously, $\psi_j = 1$. Since $\gamma_j > 0$, $\mathbf{Q}_{11}$ is stable, if and only if $\mathbf{F}$ is stable. Therefore, we can focus on the stability of $\mathbf{F}$.

A. Necessary-and-Sufficient Conditions

The eigenvalues of $\mathbf{F}$ are the roots of the characteristic polynomial

$$\lambda^3 - \mathrm{tr}(\mathbf{F})\lambda^2 + \frac{1}{2}(\mathrm{tr}(\mathbf{F})^2 - \mathrm{tr}(\mathbf{F}^2))\lambda - \det(\mathbf{F}) = 0$$

where tr and det are, respectively, the trace and the determinant of a matrix. The necessary and sufficient conditions for the roots of the polynomial to have negative real part are obtained from the Routh–Hurwitz theorem

$$\begin{aligned} \mathrm{tr}(\mathbf{F}) &< 0 \\ \mathrm{tr}(\mathbf{F}^2) - \mathrm{tr}(\mathbf{F})^2 &< 0 \\ \det(\mathbf{F}) &< 0 \\ \mathrm{tr}(\mathbf{F})(\mathrm{tr}(\mathbf{F})^2 - \mathrm{tr}(\mathbf{F}^2)) - 2\det(\mathbf{F}) &< 0. \end{aligned}$$

The necessary-and-sufficient conditions can be used to test the stability of the servoing and to obtain the robustness domain (see, e.g., the simulations in Section IV). However, for a large number of parameters, the computation time can be high. In some cases, it is preferable to have a simple test in order to know, given a bound on the precision of depths estimates $|\psi_i| \leq \overline{\psi}_i$, if the eigenvalues are negative. Similar to [29], we can also find simple sufficient conditions in order to obtain an approximation of the robustness domain.

B. Sufficient Conditions

Since $\psi_j = 1$, we can rewrite the (3×3) matrix $\mathbf{F}$ as

$$\mathbf{F} = -\widehat{\mathbf{A}}_j^{\natural}\widehat{\mathbf{A}}_j - \sum_{i=1, i\neq j}^{n} \psi_i \widehat{\mathbf{A}}_i^{\natural}\widehat{\mathbf{A}}_i$$

from equation $\widehat{\mathbf{A}}_j^{\natural}\widehat{\mathbf{A}}_j = \mathbf{I} - \sum_{i=1, i\neq j}^{n} \widehat{\mathbf{A}}_i^{\natural}\widehat{\mathbf{A}}_i$; thus

$$\mathbf{F} = -\mathbf{I} - \sum_{i=1, i\neq j}^{n} \delta_i \widehat{\mathbf{A}}_i^{\natural}\widehat{\mathbf{A}}_i = -\mathbf{I} + \mathbf{E}(\boldsymbol{\delta})$$

where $\boldsymbol{\delta} = (\delta_1, \delta_2, \ldots, \delta_m)$, and $\delta_i = \psi_i - 1$. Matrix $\mathbf{F}$ can be regarded as a perturbation of the matrix $-\mathbf{I}$, where $\mathbf{E}(\boldsymbol{\delta})$ is the

perturbation matrix. Let us define the spectral variation of a matrix $\tilde{\mathbf{m}}$ with respect to a matrix $\mathbf{m}$ as [33]

$$\mathrm{sv}_{\mathbf{m}}(\tilde{\mathbf{m}}) = \max_i \min_j |\tilde{\lambda}_i - \lambda_j|.$$

The Bauer–Fike theorem [33] states that

$$\mathrm{sv}_{\mathbf{m}}(\tilde{\mathbf{m}}) \leq \|\tilde{\mathbf{m}} - \mathbf{m}\|.$$

In our case, applying the Bauer–Fike theorem to the spectral variation $\mathbf{F}$ with respect to $-\mathbf{I}$, we obtain

$$\mathrm{sv}(\mathbf{F}) = \max_i |\tilde{\lambda}_i + 1| \leq \|\mathbf{E}(\boldsymbol{\delta})\|.$$

Thus, a simple sufficient condition for the stability of $\mathbf{F}$ is $\|\mathbf{E}(\boldsymbol{\delta})\| < 1$. Indeed, if $\|\mathbf{E}(\boldsymbol{\delta})\| < 1$, then

$$\max_i |\tilde{\lambda}_i + 1| < 1 \tag{12}$$

which implies $\tilde{\lambda}_i < 0$. From the definition of spectral variation, all others eigenvalues $\lambda_k \ \forall k$ are such that $|\tilde{\lambda}_k + 1| \leq |\tilde{\lambda}_i + 1|$. Thus, $|\tilde{\lambda}_k + 1| < 1$, which means $\tilde{\lambda}_k < 0 \ \forall k$. Now, since $\mathbf{E}(\boldsymbol{\delta}) = -\sum_{i=1, i\neq j}^{n} \delta_i \widehat{\mathbf{A}}_i^{\natural} \widehat{\mathbf{A}}_i$

$$\|\mathbf{E}\| \leq \sum_{i=1, i\neq j}^{n} |\delta_i| \|\widehat{\mathbf{A}}_i^{\natural} \widehat{\mathbf{A}}_i\|$$

and setting $\mu_i = \|\widehat{\mathbf{A}}_i^{\natural} \widehat{\mathbf{A}}_i\| > 0$, the condition (12) can be imposed by bounding the previous inequality

$$\sum_{i=1, i\neq j}^{n} \mu_i |\delta_i| < 1. \tag{13}$$

In the inequality, each error $|\delta_i|$ is weighted by the scalars μ_i. The smaller μ_i is, the larger $|\delta_i|$ can be. Thus, the best choice for the point γ_j is $\mu_j = \max_k \mu_k$. Inequality (13) defines a polygonal region whose axis are weighted by the scalars μ_i. The volume of the region $V = \prod_{i=1, i\neq j}^{n} \mu_i$ gives a measure of the robustness domain. If we suppose that the precision of measurement is the same for all points $|\delta_i| \leq \delta$, then

$$\delta < \frac{1}{\sum_{i=1, i\neq j}^{n} \mu_i}. \tag{14}$$

This is a very simple test for the local stability. Indeed, the parameters μ_i can be easily computed from image data only.

C. Special Case of Planar Targets

When the object is planar, the depths are related to the normal $\mathbf{n}$ to the plane and proportional to the distance d of the plane from the center of projection

$$Z_i = \frac{d}{\mathbf{n}^\top \mathbf{m}}$$

where $\mathbf{n} = (n_x, n_y, n_z)$ is a unit vector. This vector can be written as a function of two parameters $\mathbf{n}(\theta, \phi) = (\cos(\theta)\sin(\phi), \sin(\theta)\sin(\phi), \cos(\phi))$. The estimated depth $\widehat{Z}_i$ can be obtained using an approximation of $\widehat{\mathbf{n}}(\widehat{\theta}, \widehat{\phi})$ and $\widehat{d}$

$$\widehat{Z}_i = \frac{\widehat{d}}{\widehat{\mathbf{n}}^\top \mathbf{m}}$$

and then

$$\gamma_i = \frac{\widehat{Z}_i}{Z_i} = \frac{\widehat{d}}{d} \frac{\mathbf{n}^\top \mathbf{m}_i}{\widehat{\mathbf{n}}^\top \mathbf{m}_i} \quad \text{and} \quad \psi_i = \frac{\gamma_i}{\gamma_j} = \frac{\mathbf{n}^\top \mathbf{m}_j}{\widehat{\mathbf{n}}^\top \mathbf{m}_j} \frac{\widehat{\mathbf{n}}^\top \mathbf{m}_i}{\mathbf{n}^\top \mathbf{m}_i}.$$

As expected, the stability of the visual servoing does not depend on $\widehat{d}$ but only on $\widehat{\mathbf{n}}$.

In the particular case of a planar target, it is possible to plot for each couple $(\widehat{\theta}, \widehat{\phi})$ whether the control law is stabilizing or not. After plotting the stability regions of symmetric targets, we found the following surprising result.

Conjecture 1: If a central camera observes a centered symmetric planar target (i.e., for each point $\mathbf{m} = (x, y, 1)$, the point $\mathbf{m}' = (-x, -y, 1)$ also exists on the target) parallel to the image plane [i.e., $\mathbf{n} = (0, 0, 1)$], the control law (8) is stabilizing for any admissible choice of $\widehat{\mathbf{n}}$.

We observed this with several simulations using a pinhole or a catadioptric camera (see Section IV-B2), but we did not succeed in finding a short and elegant proof. Thus, we leave the proof to the interested reader since a symmetric planar target parallel to the image plane of a central camera is only a special configuration of the more general analysis proposed in the paper. On the other hand, in the even more particular case when the target is a square, it is possible to prove the following theorem.

Theorem 1: If a pinhole perspective camera observes a centered symmetric planar square target (i.e., the reference image consists of the four points $\mathbf{m}_1 = (-\alpha, -\alpha, 1)$, $\mathbf{m}_2 = (\alpha, -\alpha, 1)$, $\mathbf{m}_3 = (\alpha, \alpha, 1)$, and $\mathbf{m}_4 = (-\alpha, \alpha, 1)$) parallel to the image plane (i.e., $\mathbf{n} = (0, 0, 1)$), the control law (8) is stabilizing for any admissible choice of $\widehat{\mathbf{n}}$ (i.e., if $\widehat{d}\widehat{n}_z > 0$).

Proof of Theorem 1: In this simple case, we can suppose without loss of generality that $d = 1$ (we remember that the scale factor does not influence the stability), and we can explicitly compute the real part of the the eigenvalues of matrix Q_{11}

$$\mathrm{real}(\lambda_1) = \frac{-2\,\widehat{d}\,\widehat{n}_z\,\alpha^2}{\widehat{n}_x^2 + \widehat{n}_y^2 + 2\alpha^2 + 2\alpha^4(\widehat{n}_x^2 + \widehat{n}_y^2)}$$

$$\mathrm{real}(\lambda_2) = \frac{-\widehat{d}\,\widehat{n}_z((\widehat{n}_x^2 + \widehat{n}_y^2)(2\alpha^4 + 1) + 4\alpha^2)}{2\widehat{n}_z^2(\widehat{n}_x^2 + \widehat{n}_y^2)(2\alpha^4 + \alpha^2 + 1) + 2(1 + \widehat{n}_z^2)\alpha^2}$$

$$\mathrm{real}(\lambda_3) = \frac{-\widehat{d}\,\widehat{n}_z((\widehat{n}_x^2 + \widehat{n}_y^2)(2\alpha^4 + 1) + 4\alpha^2)}{2\widehat{n}_z^2(\widehat{n}_x^2 + \widehat{n}_y^2)(2\alpha^4 + \alpha^2 + 1) + 2(1 + \widehat{n}_z^2)\alpha^2}.$$

We obviously choose $\widehat{d}\widehat{n}_z > 0$ since the target must be in front of the pinhole camera (and not behind). Thus, for any admissible choice of $\widehat{\mathbf{n}}$ and for any α, the real parts of the eigenvalues are negatives, and the control law is stabilizing.

We tried to prove a similar theorem considering a centered rectangle, but it was impossible to find an easy way to show that the real part of the eigenvalues is positive. However, the simple case of the square is sufficient to support, together with the simulation (with an hyperbolic camera) presented in the following section, the claim in the conjecture. If the conjecture is proven, then we will have indications on which is the best configuration of the target so that we will have the larger stability regions.

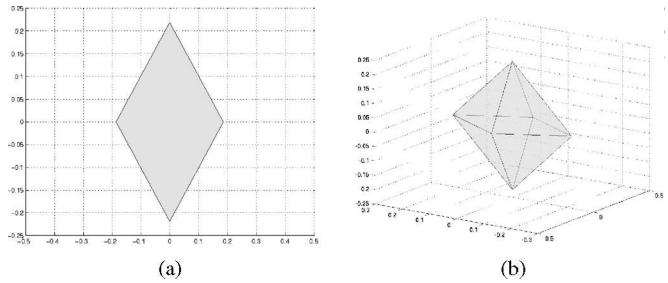

Fig. 2. Stability regions for a nonplanar object. If the parameters are chosen inside the yellow area, the control law will be stabilizing. If the parameters are chosen outside the yellow area, the control law may be stabilizing or not. (Top) Approximation of the stability region for a target composed by three points. (Bottom) Approximation of the stability region for a target composed of four points.

IV. Simulation Results

The stability results obtained in the previous section have been tested with simulations for an eye-in-hand configuration, both for planar and nonplanar targets. In this paper, we recall the results for nonplanar targets presented in [29], and we present a new set of tests with a symmetric planar target parallel to the image plane and with an ordinary planar target confirming the results obtained in [29] and [28]. As already mentioned, in this case, the stability analysis only depends on the estimated normal to the plane, whatever the number of points on the plane. Thus, from the necessary and sufficient conditions, we obtain the *exact* robustness domain.

A. Estimating the Stability Domain by the Sufficient Condition

When the target is nonplanar, it is easier to use the sufficient condition. In the simulation, we show the stability regions for 3 and 4 points since they can be represented in a plot. The 3-D point coordinates of the object were $P_1 = (-0.2, 0.2, 0.9443)$, $P_2 = (-0.2, -0.2, 0.847)$, $P_3 = (0.2, -0.2, 0.9417)$, and $P_4 = (0.2, 0.2, 0.8498)$. In Fig. 2(a), we used the first three points, and in Fig. 2(b), we used all the four points. In the first case, we find $\mu_1 = 0.186$ and $\mu_2 = 0.219$ [see Fig. 2(a)]. After adding a point not on the plane, we find $\mu_1 = 0.186$, $\mu_2 = 0.219$, and $\mu_3 = 0.223$ [see Fig. 2(b)]. For higher dimensional problems, the volume of the convex polyhedron gives an idea of the precision required in the measurement of the depth distribution.

B. Stability Domain for Planar Objects

1) Ordinary Target: Figs. 3–6 show the stability regions for conventional, parabolic, and hyperbolic cameras for an increasing number of points on the same plane. First, note that all central cameras have similar stability region. Thus, one cannot expect to increase significantly the stable region by changing the type of central camera. When considering three image points (see Fig. 3), the corresponding stable region is not so wide. Note that, adding a point inside the triangle defined by the other points (see Fig. 4) only slightly modifies the stability region. When learning the reference image, one can think that it is probably better to choose points spread in the image. If we add four more points as in Fig. 5, the clear stability region increases. Increasing then the number of points only slightly modifies the stability regions (see Fig. 6). However, even in this very favorable case, there exists an important dark instability region. Note finally that, in the three point case illustrated in Fig. 3(b), if we have absolutely no idea about the 3-D position of the plane, a simple guess $\widehat{\mathbf{n}} = (0, 0, 1)$ makes the visual servoing unstable in the case where three points are used.

2) Symmetric Target Parallel to the Image Plane: In this set of experiments, the target composed of six points is initially symmetric (with respect to the principal point) and parallel to

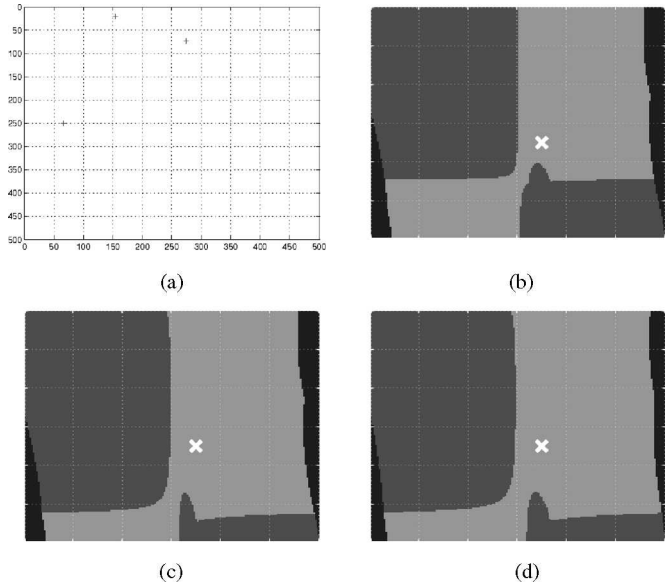

Fig. 3. (a) Image points with conventional camera; stability regions. (b) Conventional, (c) parabolic, and (d) hyperbolic cameras. If the parameters are chosen in the clear area the control law is stabilizing. If the parameters are chosen in the dark area the control law is not stabilizing. If the parameters are chosen in the black region the depth of a point is negative.

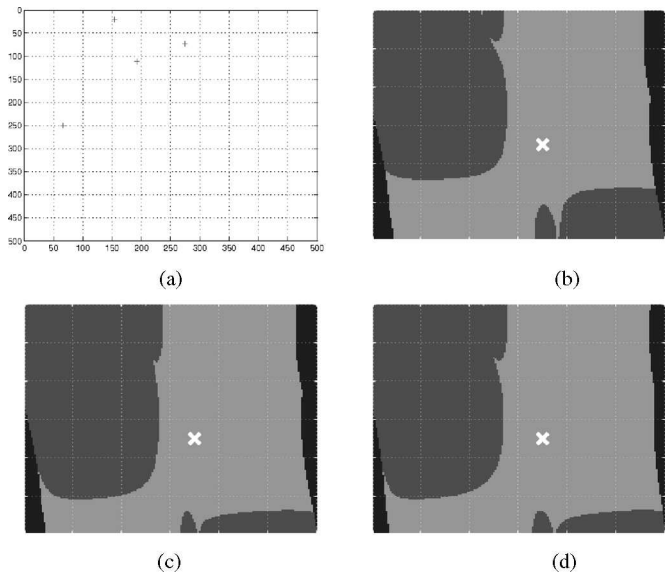

Fig. 4. (a) Image points with conventional camera; stability regions: (b) conventional, (c) parabolic, and (d) hyperbolic cameras.

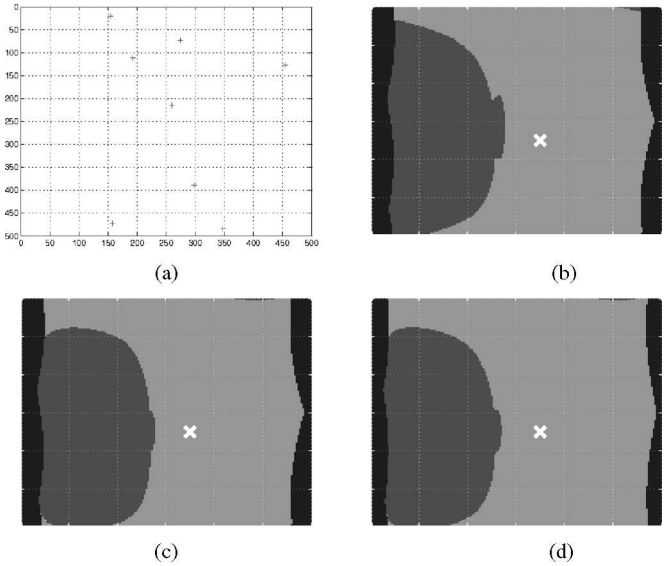

Fig. 5. (a) Image points with conventional camera; stability regions. (b) Conventional, (c) parabolic, and (d) hyperbolic cameras.

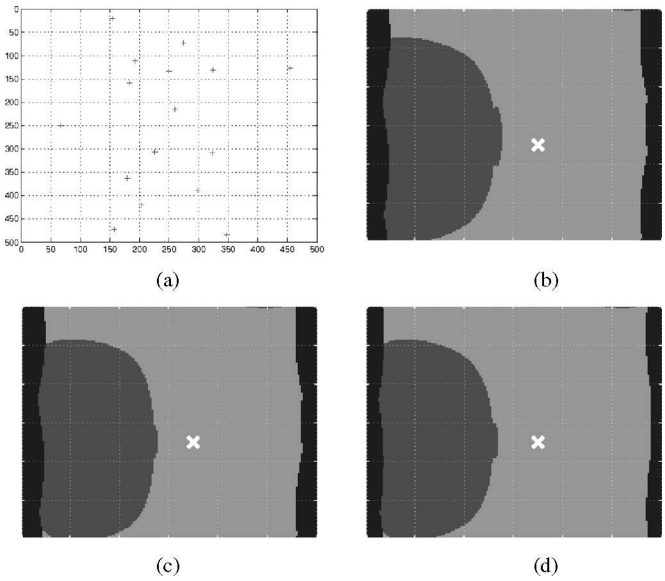

Fig. 6. (a) Image points with conventional camera; stability regions. (b) Conventional, (c) parabolic, and (d) hyperbolic cameras.

the image plane [see Fig. 7(a)]. The target is observed by a hyperbolic camera, but similar results are obtained with pinhole and parabolic cameras. The pixel coordinates of the six points are $\{(320,\ 418), (180,\ 81), (180,\ 418), (320,\ 81), (106,\ 250), (394, 250)\}$. In this case, the control law (8) is stabilizing for any admissible choice of the depth distribution, as can be seen in Fig. 7(b). The target is then slightly moved so that it no longer appeared as a symmetric target [see Fig. 7(c)–(d)]. The new image coordinates of the target are $\{(322, 422), (183, 90), (181, 414), (320, 80), (114, 250), (401, 250)\}$, and can be seen in Fig. 7(d), the unstable region is very small. The reference image is then modified in a more important manner (the new image coordinates of the target are $\{(324, 427), (190, 103), (183, 409), (317, 88), (125, 250), (394, 250)\}$; see

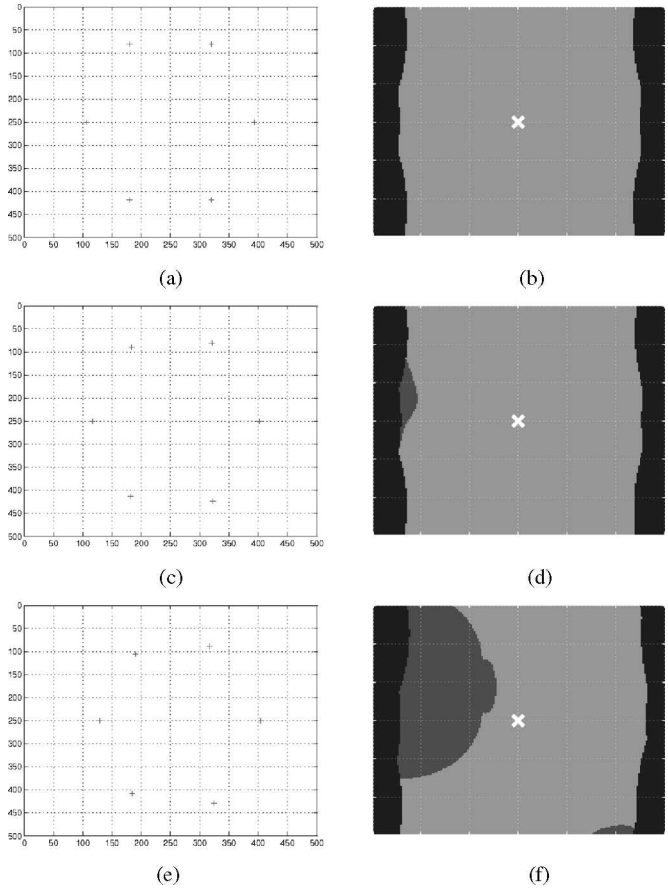

Fig. 7. (a) and (e) Image points with hyperbolic camera. (b), (d), and (f) Related stability regions.

Fig. 7(e)–(f)). As expected the unstable region increases also in a more important manner. These results confirm that a centered symmetric object parallel to the image plane is a very favorable configuration. One should, if possible, chose a configuration near this ideal one when learning the reference image.

V. Experimental Results

In this section, theoretical results are validated on a six degree-of-freedom (DOF) eye-in-hand system. A conventional calibrated perspective camera observing a planar target is used. To reduce as far as possible image processing errors, the target is composed by six white marks. The extracted visual features are the image coordinates of the center of gravity of each mark. The coordinates of these points are extracted and tracked using the visual servoing platform (VISP) library [34]. The desired depth distribution $\mathbf{z}^*$ is estimated using the nonlinear procedure presented in [35] initialized with the output of the Dementhon's algorithm [36]. The camera displacement is small and composed of a translation $\mathbf{t} = [-0.035,\ 0.004,\ 0.003]$ m and a rotation $\theta\mathbf{u} = [-1.11,\ -1.64,\ -6.97]^\circ$.

The stability regions, which are given as a function of $(\widehat{\theta},\ \widehat{\phi})$, are plotted in Fig. 8. The true normal is $\mathbf{n} = (0, 0, 1)$ and corresponds to the cross with coordinates $\theta = 0$ and $\phi = 0$ in the plot. Three experiments are presented. In the first one,

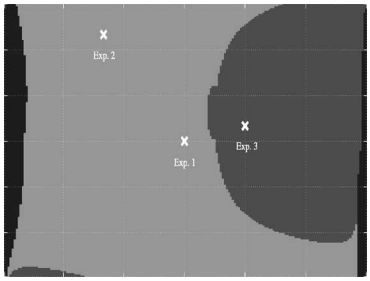

Fig. 8. Stability regions. If the parameters are chosen in the clear area, the control law is stabilizing. If the parameters are chosen in the dark area, the control law is not stabilizing. If the parameters are chosen in the black region, the depth of a point is negative, which is impossible.

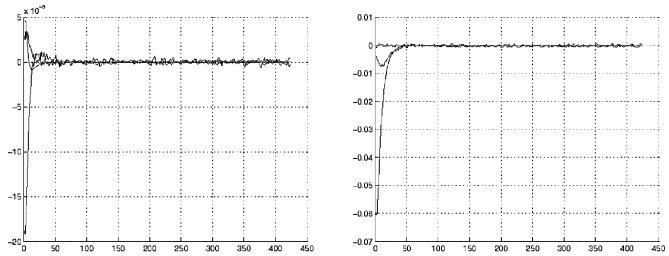

(a) (b)

Fig. 9. First experiment. The depth distribution is correct, and the control law is stable. (a) Translation velocity (in meters per second) and (b) rotation velocity (in radians per second).

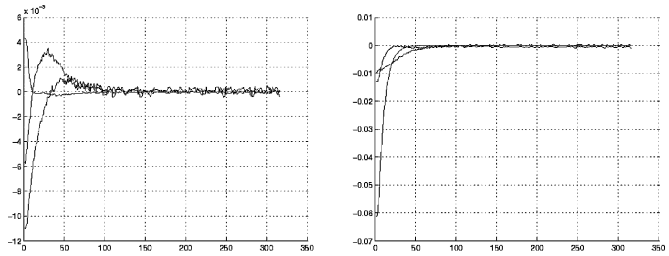

(a) (b)

Fig. 10. Second experiment. The depth distribution is not correctly estimated, and the control law is stable. (a) Translation velocity (in meters per second) and (b) rotation velocity (in radians per second).

the true depth distribution $\mathbf{z}^* = (0.912, 0.912, 0.912, 0.912, 0.912, 0.912)$m is used (corresponding to $\theta = 0$ and $\phi = 0$). In this case, as expected, the control laws is stable [see Fig. 9(a) and (b)]. In the second experiments, the depth distributions is taken as $\widehat{\mathbf{z}}^* = (1.261, 1.209, 1.162, 1.392, 1.331, 1.273)$m, which corresponds to $(\widehat{\theta}, \widehat{\phi}) = (70 \; -40)^\circ$. Once again, the control laws is stable [see Fig. 10(a) and (b)]. This was also expected since $(\widehat{\theta}, \widehat{\phi})$ lies on the stable region (the clear region in Fig. 8). In the third experiment, the depth distributions is taken as $\widehat{\mathbf{z}}^* = (0.952, 1.010, 1.077, 0.947, 1.004, 1.069)$. In this case, $(\widehat{\theta}, \widehat{\phi}) = (10\,30)^\circ$ lies on the unstable region (dark region in Fig. 8), and the control law is unstable [which is confirmed by Fig. 11(a) and (b)]. Note that, despite that the maximal and mean errors on the depth distribution is larger in the second experiment (0.480 and 0.359 m, respectively) than in the third experiment (0.165 and 0.098 m, respectively), the positioning task is correctly realized only in the second experiment.

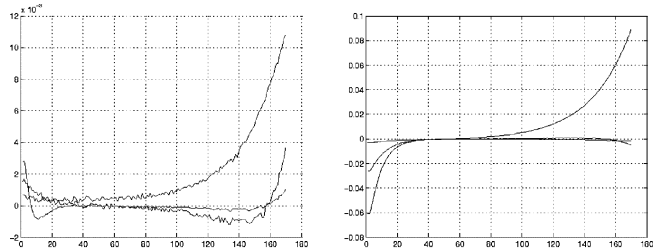

(a) (b)

Fig. 11. Third experiment. The depth distribution is not correctly estimated, and the control law is unstable. (a) Translation velocity (in meters per second) and (b) rotation velocity (in radians per second).

VI. Conclusion

In this paper, we have analyzed the robustness of image-based visual servoing with central catadioptric cameras when the 3-D parameters of a target are only approximately known. These parameters are needed to compute the control law. For all catadioptric cameras, the stability region in presence of errors on 3-D parameters can be quite large. The most favorable case is to use a pinhole camera observing in the reference image a centered symmetric object parallel to the image plane. However, in many cases, we need to take care of the instability regions since small errors on the estimated depth may lead to unstable control laws. It has been noticed that for all these sensors, the stability region is similar. Thus, one cannot expect to enlarge it by simply changing the type of central camera used. In order to improve image-based controllers, we need to study control laws that do not need the *a priori* knowledge of the 3-D parameters of the target [21], [37], [38].

Acknowledgment

The authors would like to thank the anonymous reviewers for their comments, which led them to improve and clarify the paper. In particular, the authors would like to thank the reviewer who suggested them to plot the stability domain when a planar target is a centered square, leading them to theoretically analyze that surprising particular case.

References

[1] S. Hutchinson, G. D. Hager, and P. I. Corke, "A tutorial on visual servo control," *IEEE Trans. Robot. Autom.*, vol. 12, no. 5, pp. 651–670, Oct. 1996.

[2] E. Malis, "Survey of vision-based robot control," presented at the Eur. Naval Ship Des., Captain Comput. IV Forum, Brest, France, 2002.

[3] F. Chaumette and S. Hutchinson, "Visual servo control, Part I: Basic approaches," *IEEE Robot. Autom. Mag.*, vol. 13, no. 4, pp. 82–90, Dec. 2006.

[4] F. Chaumette and S. Hutchinson, "Visual servo control, Part II: Advanced approaches," *IEEE Robot. Autom. Mag.*, vol. 14, no. 1, pp. 109–118, Mar. 2007.

[5] B. Espiau, F. Chaumette, and P. Rives, "A new approach to visual servoing in robotics," *IEEE Trans. Robot. Autom.*, vol. 8, no. 3, pp. 313–326, Jun. 1992.

[6] F. Chaumette, "Potential problems of stability and convergence in image-based and position-based visual servoing," in *The Confluence of Vision and Control,* ser. LNCIS Series vol. 237, D. Kriegman, G. Hager, and A. Morse, Eds. Berlin, Germany: Springer-Verlag, 1998, pp. 66–78.

[7] E. Malis, F. Chaumette, and S. Boudet, "2 1/2 d visual servoing," *IEEE Trans. Robot. Autom.*, vol. 15, no. 2, pp. 234–246, Apr. 1999.

[8] G. Morel, J. Szewczyk, S. Boudet, and J. Pot, "Explicit incorporation of 2d constraints in vision based control of robot manipulators," in *Proc. ISER, Exp. Robot. IV*, Sydney, Australia, 1999, vol. 2, pp. 99–108.

[9] K. Deguchi, "Optimal motion control for image-based visual servoing by decoupling translation and rotation," in *Proc. IEEE/RSJ Int. Conf. Intell. Robots Syst.*, Oct. 1998, vol. 2, pp. 705–711.

[10] E. Malis and F. Chaumette, "Theoretical improvements in the stability analysis of a new class of model-free visual servoing methods," *IEEE Trans. Robot. Autom.*, vol. 18, no. 2, pp. 176–186, Apr. 2002.

[11] H. Hadj-Abdelkader, Y. Mezouar, N. Andreff, and P. Martinet, "2 1/2 d visual servoing with central catadioptric cameras," in *Proc. IEEE/RSJ Int. Conf. Intell. Robots Syst.*, Edmonton, AB, Canada, Aug. 2005, pp. 2342–2347.

[12] P. Corke and S. Hutchinson, "A new partitioned approach to image-based visual servo control," *IEEE Trans. Robot. Autom.*, vol. 14, no. 4, pp. 507–515, Aug. 2001.

[13] K. Hashimoto and T. Noritsugu, "Enlargement of stable region in visual servo," in *Proc. IEEE Conf. Decis. Control*, Sydney, Australia, 2000, pp. 3927–3932.

[14] Y. Mezouar and F. Chaumette, "Design and tracking of desirable trajectories in the image space by integrating mechanical and visibility constraints," in *Proc. IEEE Int. Conf. Robot. Autom.*, Seoul, Korea, 2001, vol. 1, pp. 731–736.

[15] B. Espiau, "Effect of camera calibration errors on visual servoing in robotics," in *Proc. 3rd Int. Symp. Exp. Robot.*, Kyoto, Japan, 1993, pp. 183–193.

[16] C. C. Cheah, S. Kawamura, and S. Arimoto, "Feedback control for robotic manipulator with uncertain kinematics and dynamics," in *Proc. IEEE Int. Conf. Robot. Autom.*, Leuven, Belgium, May 1998, vol. 4, pp. 3607–3612.

[17] L. Deng, F. Janabi-Sharifi, and W. Wilson, "Stability and robustness of visual servoing methods," in *Proc. ICRA*, Washington, DC, 2002, vol. 2, pp. 1604–1609.

[18] R. Benosman and S. Kang, *Panoramic Vision*. Berlin, Germany: Springer Verlag, 2000.

[19] S. Baker and K. Nayar, "A theory of single-viewpoint catadioptric image formation," *Int. J. Comput. Vis.*, vol. 35, no. 2, pp. 1–22, 1999.

[20] P. Blaer and P. Allen, "Topological mobile robot localization using fast vision techniques," in *Proc. IEEE Int. Conf. Robot. Autom.*, Washington, DC, 2002, pp. 1031–1036.

[21] A. De Luca, G. Oriolo, and P. R. Giordano, "On-line estimation of feature depth for image-based visual servoing schemes," in *Proc. IEEE Int. Conf. Robot. Autom.*, 2007, pp. 2823–2828.

[22] C. Mei, E. Malis, S. Benhimane, and P. Rives, "Constrained multiple planar template tracking for central catadioptric cameras," in *Proc. Brit. Mach. Vis. Conf.*, Edinburgh, U.K., 2006, pp. 4–7.

[23] N. Winter, J. Gaspar, G. Lacey, and J. Santos-Victor, "Omnidirectional vision for robot navigation," in *Proc. IEEE Workshop Omnidirectional Vis.*, Hilton Head Island, SC, Jun. 2000, pp. 21–28.

[24] D. Burshka, J. Geiman, and G. Hager, "Optimal landmark configuration for vision based control of mobile robot," in *Proc. IEEE Int. Conf. Robot. Autom.*, Tapei, Taiwan, 2003, pp. 3917–3922.

[25] A. Paulino and H. Araujo, "Multiple robots in geometric formation: Control structure and sensing," in *Proc. Int. Symp. Intell. Robot. Syst.*, Reading, U.K., Jul. 2000, pp. 103–112.

[26] R. Vidal, O. Shakernia, and S. Sastry, "Formation control of nonholonomic mobile robots with omnidirectional visual servoing and motion segmentation," in *Proc. IEEE Int. Conf. Robot. Autom.*, Taipei, Taiwan, 2003, pp. 584–589.

[27] J. Barreto and H. Araujo, "Geometric properties of central catadioptric line images," in *Proc. Eur. Conf. Comput. Vis.*, 2002, pp. 237–251.

[28] Y. Mezouar and E. Malis, "Robustness of central catadioptric image-based visual servoing to uncertainties on 3d parameters," in *Proc. IEEE/RSJ Int. Conf. Intell. Robots Syst.*, Sendai, Japan, 2004, vol. 2, pp. 1389–1394.

[29] E. Malis and P. Rives, "Robustness of image-based visual servoing with respect to depth distribution errors," in *Proc. IEEE Int. Conf. Robot. Autom.*, Taipei, Taiwan, vol. 1, 2003, pp. 1056–1061.

[30] E. Malis, "Improving vision-based control using efficient second-order minimization techniques," in *Proc. IEEE Int. Conf. Robot. Autom.*, New Orleans, LA, Apr. 2004, vol. 2, pp. 1843–1848.

[31] C. Geyer and K. Daniilidis, "A unifying theory for central panoramic systems and practical applications," in *Proc. Eur. Conf. Comput. Vis.*, 2000, vol. 2, pp. 445–461.

[32] M. Marey and F. Chaumette, "Analysis of classical and new visual servoing control laws," in *Proc. IEEE Int. Conf. Robot. Autom.*, Pasadena, CA, May 2008, pp. 3244–3249.

[33] G. W. Stewart and J.-g. Sun, *Matrix Perturbation Theory* (ser. Computer Science and Science Computing). Orlando, FL: Harcourt Brace Jovanovich, 1990.

[34] E. Marchand, F. Spindler, and F. Chaumette, "Visp for visual servoing: A generic software platform with a wide class of robot control skills," *IEEE Robot. Autom. Mag.*, vol. 12, no. 4, pp. 40–52, Dec. 2005.

[35] E. Marchand and F. Chaumette, "Virtual visual servoing: a framework for real time augmented reality," *Comput. Graph. Forum*, vol. 21, no. 3, pp. 289–298, 2002.

[36] D. Dementhon and L. Davis, "Model-based object pose in 25 lines of code," *Int. J. Comput. Vis.*, vol. 15, no. 1–2, pp. 123–141, Jun. 1995.

[37] S. Benhimane and E. Malis, "Homography-based 2d visual tracking and servoing," *Int. J. Robot. Res.*, vol. 26, no. 7, pp. 661–676, Jul. 2007.

[38] H. Wang, Y. H. Liu, and D. Zhou, "Adaptive visual servoing using point and line features with an uncalibrated eye-in-hand camera," *IEEE Trans. Robot.*, vol. 24, no. 4, pp. 843–857, Aug. 2008.

Ezio Malis received the Bachelor's degree from the University Politecnico di Milano, Milano, Italy, and from Ecole Supérieure d'Electricité, Paris, France, in 1995 and the Ph.D. degree from the University of Rennes, Rennes, France, in 1998.

He was a Research Associate with the University of Cambridge, Cambridge, U.K., for two years. He joined the Institut National de Recherche en Informatique et en Automatique, Sophia Antipolis, France, in 2000 as a Research Scientist. His current research interests include automatics, robotics, computer vision, and, in particular, vision-based control.

Dr. Malis received the IEEE King-Sun Fu Memorial Best TRANSACTIONS Paper Award and the IEEE Wegbreit Best Vision Paper Award in 2002.

Youcef Mezouar was born in Paris, France, in 1973. He received the Ph.D. degree in computer science from the University of Rennes, Rennes, France, in 2001.

He was a Postdoctoral Associate with the Robotics Laboratory, Computer Science Department, Columbia University, New York, NY, for one year. He joined the Robotics and Vision Group, Laboratory of Sciences and Materials for Electronics, and of Automatic, University Blaise Pascal, Aubiere, France in 2002, where he is currently the Head of the Robotic and Autonomous Complex System Group. His research interests include robotics and computer vision, especially visual servoing and mobile robotic navigation.

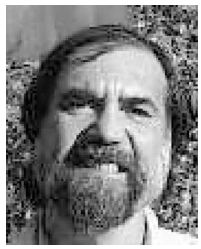

Patrick Rives (M'04) received the Doctorat de 3ième cycle degree in robotics from the Université des Sciences et Techniques du Languedoc, Montpellier, France, in 1981 and the "Habilitation à diriger les recherches" degree in 1991.

He was a Research Fellow with the Institut National de la Recherche Scientifique (INRS) Laboratory, Montreal, QC, Canada, for one year. He joined the Institut National de Recherche en Informatique et en Automatique, Rennes, France, in 1982. He is currently a Research Director with the Institut National de Recherche en Informatique et en Automatique, Sophia-Antipolis, France. His research interests include mobile robot navigation, simultaneous localization and mapping, visual servoing, sensing and scene modeling, and sensor-based control.